Journal of Solid State Chemistry 184 (2011) 273–279

Contents lists available at ScienceDirect

Journal of Solid State Chemistry

journal homepage: www.elsevier.com/locate/jssc

Improved conversion efficiency in dye-sensitized solar cells based on electrospun Al-doped ZnO nanofiber electrodes prepared by seed layer treatment

Sining Yun [a,*], Sangwoo Lim [b]

[a] School of Material Science and Engineering, Xi'an University of Architecture and Technology, Xi'an 710055, China
[b] Department of Chemical and Biomolecular Engineering, Yonsei University, Seoul 120-749, South Korea

ARTICLE INFO

Article history:
Received 20 September 2010
Received in revised form
18 November 2010
Accepted 28 November 2010
Available online 3 December 2010

Keywords:
AZO nanofibers
Electrospinning
Dye-sensitized solar cells
AZO seed layer

ABSTRACT

The application of electrospun nanofibers in electronic devices is limited due to their poor adhesion to conductive substrates. To improve this, a seed layer (SD) is introduced on the FTO substrate before the deposition of the electrospun composite nanofibers. This facilitates the release of interfacial tensile stress during calcination and enhances the interfacial adhesion of the AZO nanofiber films with the FTO substrate. Dye-sensitized solar cells (DSSC) based on these AZO nanofiber photoelectrodes have been fabricated and investigated. An energy conversion efficiency (η) of 0.54–0.55% has been obtained under irradiation of AM 1.5 simulated sunlight (100 mW/cm^2), indicating a massive improvement of η in the AZO nanofiber film DSSCs after SD-treatment of the FTO substrate as compared to those with no treatment. The SD-treatment has been demonstrated to be a simple and facile method to solve the problem of poor adhesion between electrospun nanofibers and the conductive substrate.

1. Introduction

The dye-sensitized solar cell (DSSC), which is the most efficient and stable excitonic cell, has been widely investigated due to its low fabrication cost and relatively high efficiency compared to conventional silicon solar cells [1–4]. DSSC anodes are typically constructed of TiO_2 nanoparticle films. Zinc oxide (ZnO), with a similar band gap and comparable electron injection process to that of TiO_2, has been proven to be one of the most promising alternative photoelectrode materials for application in DSSCs [5–13]. Compared to ZnO (TiO_2) nanoparticle films, single crystals of these materials exhibit significantly faster electron transport and greater electron mobility. The faster electron transport is a result of the high electron diffusion coefficients, which will provide significant advantages to device performance. The greater electron mobility is due to the directional and uninterrupted conduction channel, which can improve the efficiency of charge collection and enable the production of optically thick cells which absorb more incident light [2–4]. In spite of the improved charge transport and the larger electron mobility, one-dimensional (1D) ZnO nanowires show a smaller total surface area for nanowire arrays, as compared with the best TiO_2 nanoparticle devices, which adsorb less dye per unit thickness of the cell and thus absorb less light and collect less charge. As a result, the energy conversion efficiency (η) of ZnO nanowire-based DSSC is typically lower [1,5].

To enhance electrical and optical properties, Al, a group III element, has been regarded as one of the most representative dopants for forming n-type ZnO with good optical quality, low resistivity, high conductance, and high crystal quality. Al-doped ZnO (AZO) nanowires are capable of reaching the highest conductivity without deterioration in optical transmission and crystallinity [14–16]. Recently, Al-doped ZnO nanorod arrays as photoelectrode has been applied to fabricate DSSC, a large increase of the η in Al-doped ZnO nanorod-based DSSCs (1.34%) as compared to undoped (0.05%) has been obtained [17].

So far, different technologies such as metal-organic chemical vapor deposition (MOCVD) [7,8], hydrothermal synthesis [5,6,12,13], vapor deposition [9,13], vapor transport [18] and electrospinning [19–21] have been employed to fabricate 1D ZnO nanostructures (wires, rods, belts, tubes and fibers). Among them, the electrospinning technique is one of the simplest, most versatile, and cost-effective approaches to the preparation of 1D ZnO nanofibers [22,23]. However, the poor adhesion of electrospun nanofibers to the substrate is a key problem, which has limited the application of electrospun nanofibers in DSSCs. To solve this problem, Liu et al. have developed a buffer layer to improve the adhesion of TiO_2 nanofibers to the substrate [24]. The buffer layer releases the tensile stress at the interface of the FTO substrate and ZnO nanofibers, which prevents the subsequent ZnO nanofibers from

* Corresponding author. Fax: +86 29 85535724.
E-mail address: alexsyun1974@yahoo.com.cn (S. Yun).

0022-4596/$ - see front matter © 2010 Elsevier Inc. All rights reserved.
doi:10.1016/j.jssc.2010.11.024

cracking or peeling off from the substrate, resulting in good adhesion of the ZnO film to the FTO substrate and giving a high efficiency of 2.58% in a ZnO nanofibrous DSSC [22]. Song et al. [23] adopted a hot press pretreatment to enhance the adhesion of the nanofiber to the substrate. A subsequent study by Kim et al. [25] employed this method to enhance the adhesion of ZnO nanofiber to the FTO substrate, and the resulting ZnO nanofiber mats have produced a device efficiency of 1.34%. Onozuka et al. [26] used a solvent vapor to relax the nanofiber mats to produce an improved adhesion of the nanofiber to the substrate.

Although these methods have improved the adhesion of electrospun nanofibers to the substrate for their application to DSSCs, it is noteworthy that the morphology of the nanofibers has been greatly modified to give the higher solar conversion efficiency. To enable practical and reproducible photovoltaic devices, the issue of good electrical contact between the nanofibers and electrodes should be properly addressed. In this regard, a simple and efficient method to solve the problem of adhesion between electrospun nanofibers and the substrate is introduced in the present research. A seed layer (SD) was prepared on the substrate using electrospining before the deposition of the electrospun composite nanofibers. Good interfacial adhesion was achieved after calcination and a DSSC based on such electrospun AZO nanofiber films was fabricated. The electrospun AZO nanofiber films were found to exhibit high solar conversion efficiency and the results are discussed.

2. Experimental procedures

2.1. Nanofiber preparation by electrospining

To prepare Al-doped ZnO (AZO) nanofibers onto a fluorine-doped tin oxide (FTO) substrate (1.5 cm × 1.5 cm), the precursor solution was firstly prepared by dissolving poly(vinyl acetate) (PVAc, MW=500,000 g/mol, Aldrich) and zinc acetate dihydrate ($Zn(CH_3COO)_2 \cdot 2H_2O$, 99.0%, Aldrich) into N,N-dimethylformamide (DMF, 99.8%, Aldrich) solution with certain amount of acetic acid as a catalyst. Aluminum nitrate nonahydrate ($Al(NO_3)_3 \cdot 9H_2O$, 99.997%, Aldrich) ranging from 0 to 6.0 mol% (the ratio of Al to ZnO) was then added to the precursor solution and stirred for 4–6 h at 60 °C to obtain a homogeneous, transparent and viscous gel. The resulting gel was delivered to a 32 gage stainless needle (inner diameter: 0.2 mm) at a constant flow rate of 60 μl min^{-1} by a syringe pump (KDS Model 200 Series, KD Scientific Inc., USA). The needle was connected to a high-voltage power supply. An electric field of 15 kV was applied between the orifice and the ground at a distance of 15 cm. AZO–PVAc composite nanofibers were collected on a piece of flat aluminum foil flattened on a laboratory jack. The thickness of the nanofiber films was controlled by the electrospinning time. The composite nanofiber films along with their substrates were then sintered at 450 °C for 1 h in air to obtain the AZO nanofiber films, with heating rates of 2 °C per minute.

2.2. DSSC fabrication

To fabricate DSSC, as-spun Al-doped ZnO nanofibers were first immersed into a 0.5 mM ethanolic solution of the dye cis-bis (isothiocyanato)bis(2,2′-bipyridyl-4,4′-dicarboxylato)-ruthenium(II) bis-tetrabutylammonium (N719) purchased from Solaronix at room temperature for 1 h. A platinized conductive oxide glass used as the counterelectrode was prepared using Pt (99.99% purity) target in Ar (99.999% purity) ambient with RF power of 100 W at room temperature at 5 mTorr. The FTO substrate with dye were next sandwiched and bonded with a sputtered Pt counterelectrode. After that, the two electrodes of the cells were sealed using 50-μm-thick hot-melt spacer (Dupont, grade 1702). Sealing was accomplishing by pressing the two electrodes together at a temperature of about 200 °C within a few seconds. Then, the redox electrolyte, consisting of 0.5 M LiI, 50 mM I_2, and 0.5 M 4-tertbutylpyridine in 3-methoxypropionitrile (Fluka), was introduced into the cell through one of the small holes drilled in the counterelectrode by capillary forces. Finally, these holes were covered and sealed with a fast-speed solidification epoxy polymer to prevent leakage of the fluid-type electrolyte. During these entire procedures, the active electrode area of the resulting cell was approximately 1 cm^2.

2.3. Characterizations

The structure and phase evolution of Al-doped ZnO nanofiber films were examined using X-ray diffraction (XRD, D/Max2200 RZGAKV: Rigaku Inc.D, Japan). Scanning electron microscope (SEM, Quanta 200 FEG System: FEI Co., USA) and field-emission scanning electron microscope (FESEM, S-4200: Hitachi, Japan) were carried out for an investigation of the development of the microstructure and morphology of the AZO nanofibers during the process steps. High resolution transmission electron microscopy (HRTEM, JEM2100: JEOL, Japan) was used to examine individual AZO nanocrystal structures. Samples for HRTEM were prepared dispersing the films of the AZO nanofibers in ethanol followed by allowing a drop of this suspension to dry on a carbon-coated Cu grid. The binding energy level and the chemical structure of Al-doped ZnO nanofiber films were measured by X-ray photoelectron spectroscopy (XPS, Multilab 2000: Thermo VG Scientific, England) with a monochromatic Al $K\alpha$ radiation source at room temperature. The device photovoltaic characteristics were measured by Sun 2000 Series Solar Simulators (ABET-Technologies, Model 11000) under white light illumination condition (Xe arc lamp, 1.5 AM, 1000 W/m^2). All the measurements were performed at room temperature.

3. Results and discussion

Fig. 1(a) and (b) shows FESEM images of the as-spun AZO–PVAc composite nanofibers. These maintain cross-sectional uniformity are smooth throughout their length and exhibit a range of diameters from 40 to 159 nm. The average diameter of the as-spun composite nanofibers, 82 ± 24 nm, was obtained from the respective diameter histogram of the as-spun AZO–PVAc composite nanofibers (see Fig. 1(d)). The size distribution of the as-spun AZO–PVAc composite nanofibers is also shown in Fig. 1(d) using 100 random nanofibers taken from the FESEM images. The electrospun AZO nanofiber films were fabricated by calcination, as shown in Fig. 1(c). The morphologies of the nanofibers are shown to have changed from a relatively smooth and uniform fiber to a linked-crystallite particulate form, which is probably due to the decomposition of residual organics and crystallization during the calcination process. In addition, strong stresses generated due to the calcination process lead to the shrinkage and roughness of the AZO nanofiber films, which will also play a vital role in the change of properties of the nanofibers.

Structural identification of the electrospun AZO nanofibers was carried out using XRD in the range of 2θ between 20° and 60°, as shown in Fig. 2. The result indicated that the electrospun AZO nanofibers calcined at 450 °C had polycrystalline structures consisting of a wurtzite ZnO (JCPDS: 36-1451) phase characterized with primary (100), (002), and (101) peaks, suggesting that Al was incorporated homogeneously into the ZnO matrix. Based on the XRD information, the lattice parameters, a=0.3243 nm and c=0.5230 nm, were calculated from diffraction peaks using MDI Jade 5.0 software. The size of crystallites in the sample was also estimated from the highest intensity peak (101) using the Scherrer

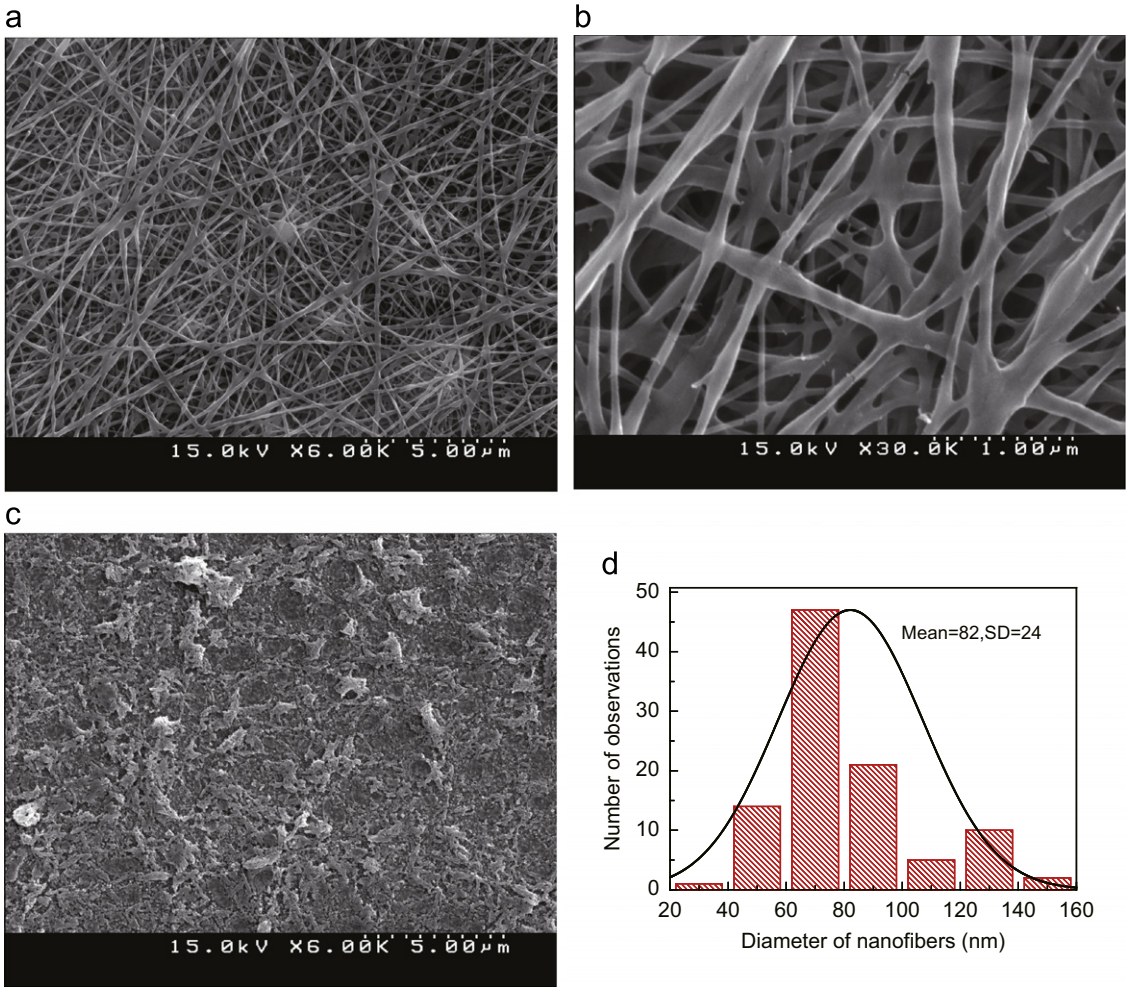

Fig. 1. (a) Low and (b) high magnification FESEM images of the as-spun AZO–PVAc composite nanofibers. (c) FESEM images of AZO nanofiber films after calcinations at 450 °C. (d) Histogram for size distribution of the as-spun AZO–PVAc composite nanofibers in Fig. 1(b).

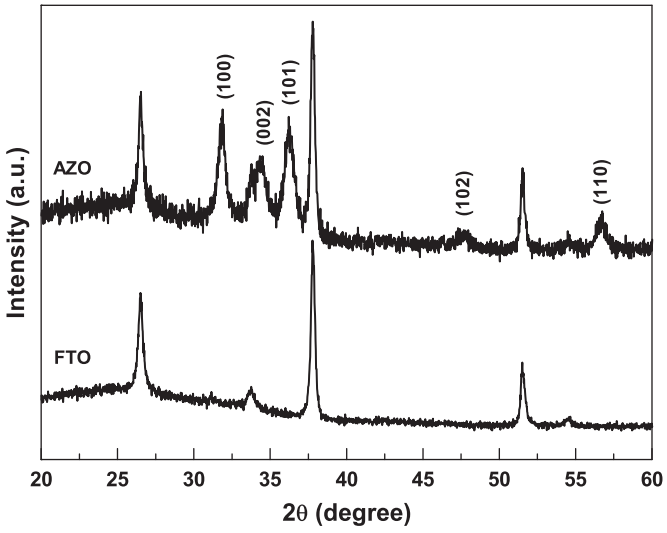

Fig. 2. XRD patterns of AZO nanofibers calcined at 450 °C. The peak of FTO substrate is also given here.

equation:

$$D = 0.89\lambda/(\beta \times \cos\theta) \quad (1)$$

where D is the crystallite size, λ is the wavelength of incident X-ray, θ is the Bragg angle of the diffraction line, and β is the FWHM in radians. The AZO nanofiber films exhibited an average grain size of approximately 20 nm.

To analyze the elemental and chemical-state of the AZO nanofibers, XPS measurements were employed. The peaks located at 1021.60 eV (Zn 2*p*3/2) and at 1044.70 eV (Zn 2*p*1/2) were observed, as can be seen in Fig. 3(a) for the AZO. There is no significant difference in the chemical shift and signal for Zn 2*p*3/2 and Zn 2*p*1/2. The atomic concentrations of Al obtained from the XPS data is 2.48 at%. Al 2*p* peaks are located at 74.70 eV for the AZO (see Fig. 3(b)). The appearance of the Al peaks in the AZO nanofiber films indicates that Al has been successfully doped into the ZnO lattice and an Al–O bond has been formed at the interface region of ZnO.

Usually, the typical O 1*s* peaks on the surface of ZnO can be fitted from high binding energy to low binding energy using three Gaussian components. The component on the highest binding energy side of the O 1*s* spectrum can be ascribed to the presence of specific chemisorbed oxygen such as the adsorbed H_2O, O_2 and $-CO_3$ [27–29]. The component with medium binding energy is related to the oxygen ions in the oxygen-deficient regions within the matrix of ZnO [30,31], whose intensity partly represents the variation in the concentration of oxygen vacancies. The component on the lower binding energy side of the O 1*s* spectra is attributed to the oxygen ions in the ZnO lattice. It can be found from Fig. 3(c) that the O 1*s* peak has been fitted by four nearly Gaussian distributions

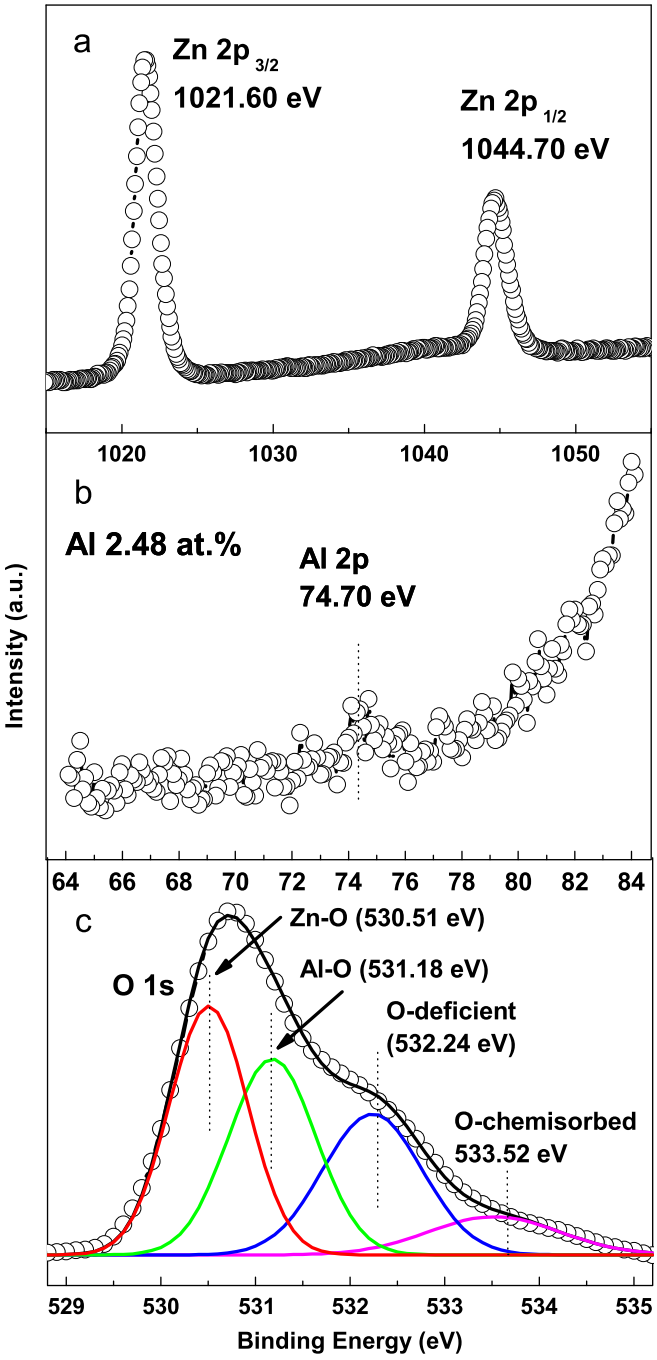

Fig. 3. XPS spectra of electrospun AZO nanofiber films calcined at 450 °C: (a) Zn 2*p*3/2 and Zn 2*p*1/2 spectra, (b) Al 2*p* spectrum and (c) O 1*s* spectrum (open circle: experimental data; solid line: fitting data).

for the AZO nanofiber film samples. Each resolved component has a full width at half maximum (FWHM) of less than 2.00 eV. Previous reports have demonstrated that the binding energy of Al_2O_3 is higher than that of ZnO [32,33], that is, the location of the O 1*s* peak in Al_2O_3 is at higher binding energy than that of ZnO. In the present research, each O 1*s* peak at 531.18 eV results from the Al–O bond, while the O 1*s* peaks at 530.51 eV are from the Zn–O bond, which is a characteristic of oxygen ions on the wurtzite structure of a hexagonal zinc ion array.

To obtain AZO nanofiber, the as-spun AZO–PVAc composite nanofibers containing the organic matrix polymer and inorganic precursors must be calcined, and thus the residual organic components are decomposed. Due to the high temperature used for the calcination process, strong stresses are generated, which leads to the shrinkage and roughness of the AZO nanofiber films, as shown in Fig. 4(a) and (b). Moreover, calcination causes the AZO nanofibers to crack and peel away from the FTO substrates. In addition, the AZO nanofiber films exhibit poor adhesion to the FTO substrate, which can clearly be seen from the images of the AZO in Fig. 4(c) and (d). Such shrinkage effects and poor adhesion limit the application of the electrospun nanofiber films, especially for photovoltaic devices like DSSCs.

For DSSCs based on electrospun AZO nanofibers, it is necessary to deposit the nanofibers onto the FTO substrates. However, the as-spun composite nanofibers can easily crack and peel away from the substrate after calcination due to the shrinking effect and poor adhesion, as previously reported for ZnO films [34]. To solve this problem, a seed layer (SD) can be introduced to improve the adhesion of the AZO nanofiber film to the FTO substrate. The precursor solution containing aluminum nitrate, as described in the experimental procedure, was initially coated on to the FTO substrate by the electrospining technique before the deposition of the electrospun composite nanofibers. Subsequently, the sample was heated rapidly to 450 °C for 30 min in air, with heating rates of 10 °C per minute, and thus the residual organics were decomposed and a AZO seed layer was spontaneously formed on the FTO substrate. The resulting substrates were then placed on a hotplate at 60 °C, Finally, the electrospun AZO–PVAc composite nanofibers were directly deposited on to the SD-treated FTO substrate. By such a simple and reliable method, a seed layer is formed spontaneously between the AZO fiber films and the FTO substrate, which facilitates the release of interfacial tensile stress during calcination and prevents the subsequent AZO nanofiber films cracking or peeling away from the substrate. As a result, the problem of poor adhesion between the AZO nanofibers and the FTO substrate was effectively solved.

Fig. 5(a) and (b) shows SEM images of the AZO nanofiber films on the SD-treated FTO substrate. Compared with Fig. 1(c) and Fig. 4(c), (d), the SD-treatment has greatly improved the interfacial adhesion of the AZO nanofiber films to the FTO substrate; the electrospun AZO nanofiber films did not crack and peel away from the substrate after calcination. To investigate further individual single grains of the AZO nanofiber films, a TEM analysis was carried out. Fig. 5(c) and (d) shows bright-field TEM images of the AZO nanofiber films. The calcined AZO nanofibers have a linked-crystallite particulate form and consisted of individual AZO single grains with size distributions of 15–48 nm. The estimated average grain size from the TEM images is 29 ± 7 nm. The size distribution is well matched to that based on the Scherrer equation using data from the XRD pattern.

Photovoltaic devices based on such fibrous films were also investigated. Fig. 6 shows photocurrent density vs. voltage characteristics of the dye-sensitized AZO electrodes under AM 1.5 G light illumination. The photovoltaic characteristics of DSSC based electrospun AZO nanofiber electrodes are listed in Table 1. *FF*, V_{oc} and J_{sc} are the fill factor, open circuit photovoltage and short-circuit photocurrent, respectively. From Table 1, it can be seen that Devices A and B, based on the AZO nanofiber films deposited directly on the FTO substrate, show poor energy conversion efficiencies (η), 0.03–0.04%, which can be attributed to the poor adhesion of electrospun nanofibers to the FTO substrate due to nanofibers cracking and peeling away from the substrate after calcination (see also Fig. 4(c) and (d)). Following SD-treatment to the FTO substrate, the adhesion of the AZO nanofiber films to the FTO substrate has been greatly improved, as shown in Fig. 6 and Table 1. An energy conversion efficiency (η), 0.54–0.55%, was obtained for Device A-SD and Device B-SD, indicating a massive increase of η in the AZO nanofiber film based DSSC after SD-treatment. The improved cell performance is mainly attributed

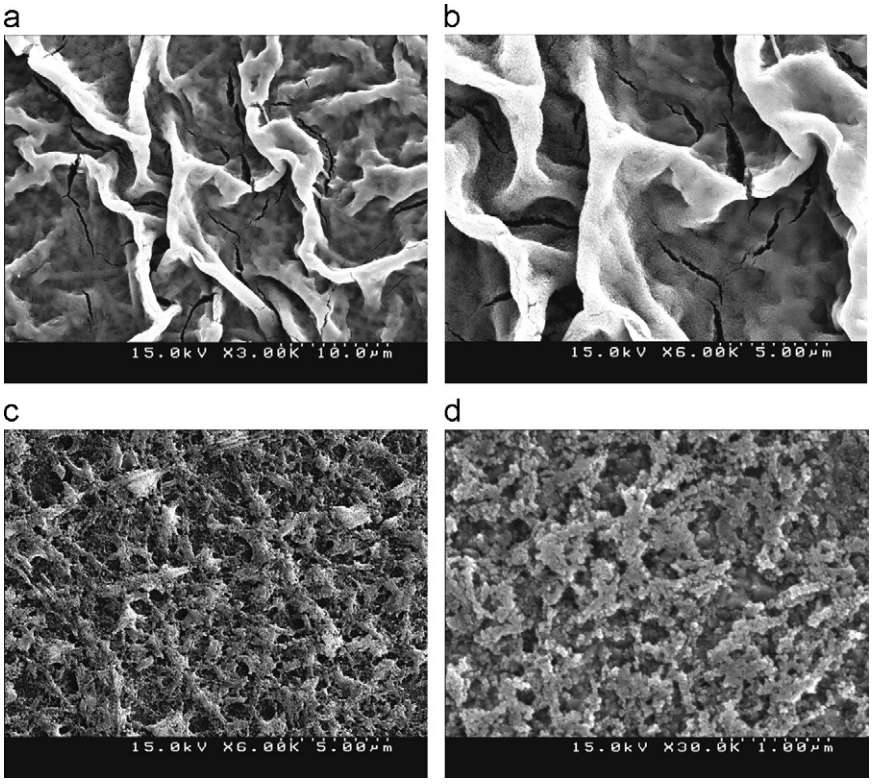

Fig. 4. (a) Low and (b) high magnification FESEM images of AZO nanofiber films that shrunk due to strong stresses generated during calcination process. (c) Low and (d) high magnification FESEM images of AZO nanofiber films that cracked and peeled off on the substrate after calcination due to the shrinking effect and poor adhesion.

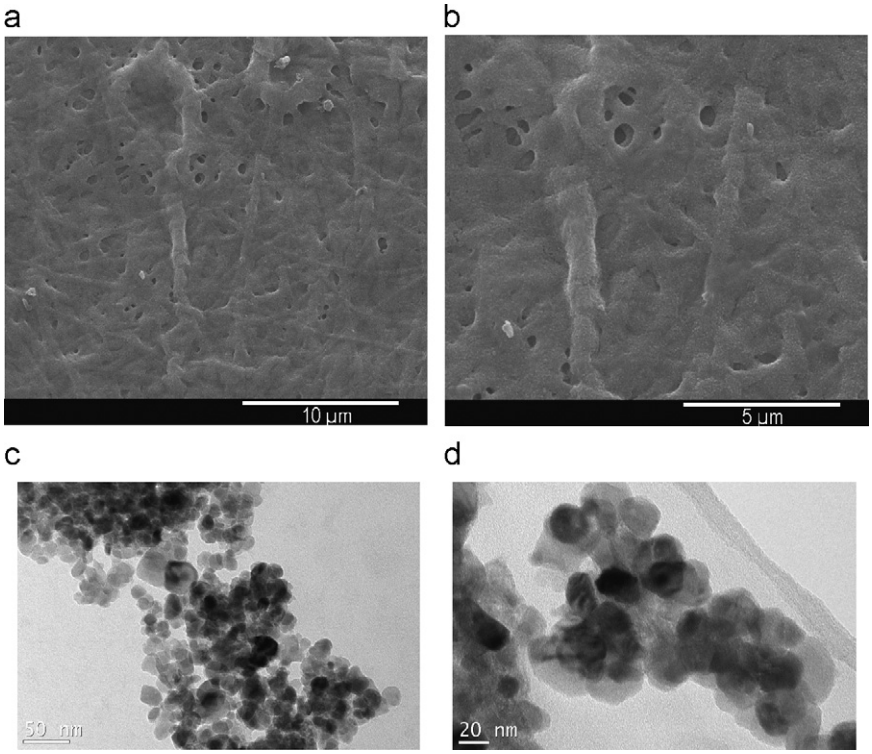

Fig. 5. (a) Low and (b) high magnification SEM images of AZO nanofiber films on the SD-treated FTO substrate. (c) Low and (d) high magnification bright-field TEM images of AZO nanofiber films composed of single crystalline grains of 15–48 nm in diameter.

to the improvement in short-circuit photocurrent J_{sc} and open circuit photovoltage V_{oc}, which can be basically attributed to the good electrical contact between the nanofibers and electrodes.

An one-diode equivalent circuit model of the DSSC has demonstrated that the shunt resistance (R_{sh}) and the series resistance (R_s) have an impressive effect on solar cells characteristics of the

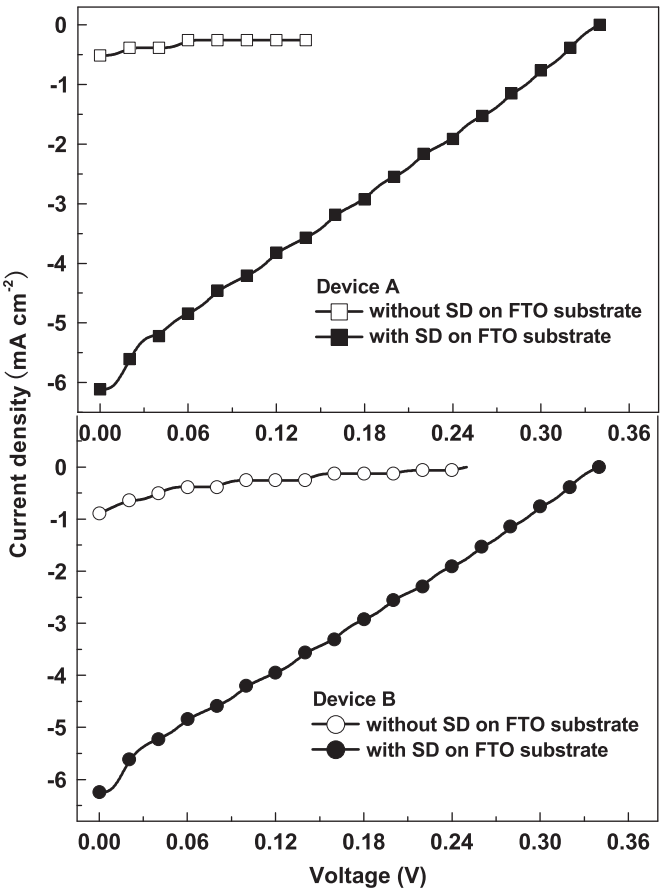

Fig. 6. Photocurrent density vs. voltage characteristics of a DSSC based on electrospun AZO nanofiber films on the FTO substrate with and without SD-treatment.

Table 1
Parameters of AZO nanofiber films-based DSSC.

Device	J_{sc} (mA cm^{-2})	V_{oc} (V)	*FF*	η (%)
A	**0.4597**	**0.2812**	**0.2620**	**0.03**
A-SD	**6.2420**	**0.3338**	**0.2574**	**0.54**
B	**0.6266**	**0.2255**	**0.2569**	**0.04**
B-SD	**6.3410**	**0.3336**	**0.2587**	**0.55**

devices [7,35]. Generally, high series resistance and low shunt resistance will deteriorate the performance of the DSSC. R_{sh} is due to the leakage path across the dye/oxide interface, induced by defects in the bulk and at the surface of the oxide. R_s is mainly attributed to the bulk resistance of semiconductor oxide films, TCO electrode, metallic contacts and electrolyte [7]. In the present research, the SD-treatment employed has greatly improved the adhesion of the electrospun nanofibers to the FTO substrate, which may induce a strong decrease in R_s and increase in R_{sh}, and leads to the improvement of cell performance in Device A-SD (Device B-SD), that is, the increased V_{oc} and J_{sc}, as compared with Device A (Device B). It is reasonable to believe that the modified adhesion between electrospun nanofibers and the conductive substrate should be responsible for the improved R_s and R_{sh} in DSSC. Further better photovoltaic device performance can be expected by optimizing the properties of the AZO nanofibers such as dimension, doping level and crystal phase.

4. Conclusions

In conclusion, photovoltaic devices based on electrospun AZO nanofibrous films are demonstrated. To improve the poor adhesion between electrospun nanofibers and the conductive substrate, a seed layer (SD) was introduced as a buffer layer to facilitate the release of interfacial tensile stress during calcination and enhance the interfacial adhesion of the AZO nanofiber films with the FTO substrate. Unique morphology of the AZO nanofiber films after calcination is a linked-crystallite particulate form and composed of individual AZO single grains with size distributions of 15–48 nm. The estimated average grain size from the TEM is 29 ± 7 nm. Dye-sensitized solar cells (DSSC) based on the AZO nanofiber photoelectrodes give a total energy conversion efficiency of 0.54–0.55% under irradiation of AM 1.5 simulated sunlight with a power density of 100 mW/cm^2 indicating a massive improvement of η in the AZO nanofiber film DSSCs after SD-treatment of the FTO substrate as compared to those with no treatment. A SD-treatment, it has been demonstrated, is a simple and facile method to solve the problem of poor adhesion between electrospun nanofibers and the conductive substrate.

Acknowledgments

The authors acknowledge the financial support of the Foundation of the Education Ministry of Shaanxi Province under Grant No. 2010JK655. This work was also supported by the Project of Science and Technology for Returned Overseas Research Fellow through Shaanxi Administration of Foreign Expert Affairs. The Project-sponsored by SRF for ROCS, SEM. The authors are grateful to Jing Shi for the contribution to TEM measurement.

References

[1] A. Hochbaum, P. Yang, Chem. Rev 110 (2010) 527–546.
[2] V. Noack, H. Weller, A. Eychmuller, J. Phys. Chem. B 106 (2002) 8514–8523.
[3] P. Wagner, R. Helbig, J. Phys. Chem. Solids 35 (1974) 327–335.
[4] D. Thomas, J. Lander, J. Chem. Phys. 25 (1956) 1136–1142.
[5] M. Law, L. Greene, J. Johnson, R. Saykally, P. Yang, Nat. Mater. 4 (2005) 455–459.
[6] Y. Gao, M. Nagai, T. Chang, J. Shyue, Cryst. Growth Des. 7 (2007) 2467–2471.
[7] H. Chen, A. Pasquier, G. Saraf, J. Zhong, Y. Lu, Semicond. Sci. Technol. 23 (2008) 045004.
[8] J. Baxter, E. Aydil, Appl. Phys. Lett. 86 (2005) 053114.
[9] B. Pradhan, S. Batabyal, A. Pal, Sol. Energy Mater. Sol. Cells 91 (2007) 769–773.
[10] K. Keis, E. Magnusson, H. Lindström, S. Lindquist, A. Hagfeldt, Sol. Energy Mater. Sol. Cells 73 (2002) 51–58.
[11] E. Hosono, S. Fujihara, I. Honma, H. Zhou, Adv. Mater. 17 (2005) 2091–2094.
[12] L. Greene, M. Law, D. Tan, M. Montano, J. Goldberger, G. Somorjai, P. Yang, Nano Lett. 5 (2005) 1231–1236.
[13] Y. Hsu, Y. Xi, A. Djuriši, W. Chan, Appl. Phys. Lett. 92 (2008) 133507.
[14] R. Wang, C. Liu, J. Huang, S. Chen, Appl. Phys. Lett. 88 (2006) 023111.
[15] X. Xue, L. Li, H. Yu, Y. Chen, Y. Wang, T. Wang, Appl. Phys. Lett. 89 (2006) 043118.
[16] C. Hsu, S. Chang, H. Hung, Y. Lin, C. Huang, Y. Tseng, I. Chen, J. Electrochem. Soc. 152 (2005) G378–G381.
[17] S. Yun, J. Lee, J. Chung, S. Lim, J. Phys. Chem. Solids 71 (2010) 1724–1731.
[18] M. Huang, Y. Wu, H. Feick, N. Tran, E. Weber, P. Yang, Adv. Mater. 13 (2001) 113–116.
[19] D. Lin, H. Wu, W. Pan, Adv. Mater. 19 (2007) 3968–3972.
[20] D. Li, Y. Xia, Nano Lett. 3 (2003) 555–560.
[21] R. Ramaseshan, S. Sundarrajan, R. Jose, S. Ramakrishna, J. Appl. Phys. 102 (2007) 111101.
[22] W. Zhang, R. Zhu, X. Liu, B. Liu, S. Ramakrishna, Appl. Phys. Lett. 95 (2009) 043304.
[23] M. Song, D. Kim, K. Ihn, S. Jo, D. Kim, Nanotechnology 15 (2004) 1861.
[24] R. Zhu, C. Jiang, X. Liu, B. Liu, A. Kumar, S. Ramakrishna, Appl. Phys. Lett. 93 (2008) 013102.
[25] I. Kim, J. Hong, B. Lee, D. Kim, E. Jeon, D. Choi, D. Yang, Appl. Phys. Lett. 91 (2007) 163109.
[26] K. Onozuka, B. Ding, Y. Tsuge, T. Naka, M. Yamazaki, S. Sugi, S. Ohno, M. Yoshikawa, S. Shiratori, Nanotechnology 17 (2006) 1026.
[27] M. Chen, X. Wang, Y. Yu, Z. Pei, X. Bai, C. Sun, R. Huang, L. Wen, Appl. Surf. Sci. 158 (2000) 134–140.

[28] S. Major, S. Kumar, M. Bhatnagar, K. Chopra, Appl. Phys. Lett. 49 (1986) 394–396.
[29] M. Islam, T. Ghosh, K. Chopra, H. Acharya, Thin Solid Films 280 (1996) 20–25.
[30] T. Szörényi, L. Laude, I. Bertóti, Z. Kántor, Z. Geretovszky, J. Appl. Phys. 78 (1995) 6211–6219.
[31] J. Fan, J. Goodenough, J. Appl. Phys. 48 (1977) 3524–3531.
[32] K. Han-Ki, T. Seong, K. Koung-Kook, P. Seoug-Ju, Y. Yoon, I. Adesida, Jpn. J. Appl. Phys. 43 (2004) 976–979.
[33] S. Yun, J. Lee, J. Yang, S. Lim, Physica B 405 (2010) 413–419.
[34] Y. Deesirapipat, M. Fujita, M. Sasajima, R. Suzuki, C. Antarasena, Y. Horikoshi, Jpn. J. Appl. Phys. 44 (2005) 5150–5155.
[35] J.C. Bernède, L. Cattin, M. Morsli, Y. Berredjem, Sol. Energy Mater. Sol. Cells 92 (2008) 1508–1515.